ELSEVIER

Journal of Molecular Graphics and Modelling 21 (2002) 101–110

Journal of Molecular Graphics and Modelling

www.elsevier.com/locate/JMGM

Geometrical modelling of Ohmic conductance in ion channels

Jeffrey Sutherland, Gustavo A. Arteca*

Département de chimie et biochimie, Laurentian University, Sudbury, Ontario, Canada P3E 2C6.

Received 11 April 2002

Abstract

In an Ohmic model, channel conductivity can be described in terms of the geometry of a conducting cable. The essential features of such devices are the arc length of the curve describing the channel's longitudinal path, and the cross-sectional areas transversal to this curve. In a first approximation, conducting channels can be represented by an average molecular shape with estimated lengths and cross-sectional areas. Whereas the physical shortcomings of this approach are known, its accuracy limitations in practice have not been established. In this work, we discuss an improved model for the channel's shape, one that allows us to gauge how much of the Ohmic conductivity can be assigned purely to geometrical features. In the present algorithm, we investigate all regions inside the pore that are accessible to ions using various choices for the molecular surface of the inner channel. We discuss the agreement with experimental conductances in the case of 12 channels (cholera toxin B-subunit pentamer, *Staphylococcus aureus* α-hemolysin, *Streptomyces lividans* KcsA channel, seven porins, gramicidin A, and phospholamban). Our results can be regarded as a benchmark for the best performance that can be expected from a geometrical model of conductance. Consequently, significant deviations from experimental trends can safely be assigned to *non-geometrical* factors, namely the specific composition of the ion channel and the detailed electrostatic interactions between the channel and a particular ion.

Keywords: Conductance; Cell constant; Transport channels; Gramicidin; Porins

1. Introduction

Cellular channels are an important class of membrane-bound proteins which allow the passage of selected molecules and ions across the otherwise impermeable phospholipid bilayer. Channels may exist permanently on the membrane, however other proteins can occasionally insert themselves and function as channels. Some antibiotics and toxins (e.g. gramicidin A and the bacterial α-hemolysin) belong to the latter class. Some channels regulate the transport by modulating the transmembrane electric potential. Presently, we consider membrane channels that allow the *passive* transport of ions and solvent. As a working hypothesis, we can initially assume that the key feature regulating this transport is the *channel's shape*. In this work, we test the limitations of this hypothesis by using an improved model for the *geometrical contribution to ion channel conductance*.

Due to the difficulties in solubilization and crystallization, membrane proteins are less well characterized experimentally than other proteins [1]. Theoretical modelling provides an alternative to understand some of their structural and functional features [2,3]. Molecular dynamics and Monte Carlo simulations cast light on the conduction mechanism, but at considerable computational cost. Alternative algorithms have thus been proposed, seeking to obtain qualitative estimates of key physical properties of protein channels, with a minimum effort at representing the force fields describing the channel and membrane environment.

In this work, we discuss some improvements on earlier methods developed for the fast calculation of the geometric contribution to the Ohmic conductance of ion channels [4–6]. Within this approach, we incorporate many details of the local geometrical features of a hard-sphere model of a channel, using the available structural information (NMR, X-ray or theoretical model). In the next two sections, we discuss the underlying theory and the implementation of the algorithms. A following section uses the algorithms for estimating channel conductances; results are compared with experimental trends. The final section discusses the usefulness and limitations of the model, and addresses the reasons for the observed deviations.

2. General methodology

The channels studied in this work exhibit a longitudinal cavity (or "pore"); it allows ion translocation in a

* Corresponding author.
E-mail address: gustavo@laurentian.ca (G.A. Arteca).

1093-3263/02/$ – see front matter
PII: S1093-3263(02)00126-2

hydrophilic environment, and it may also be filled with solvent molecules. This pore lends itself to modelling its conductance by using an Ohmic model, i.e. one where the geometry of the pore is used to calculate the cell constant, K_{cell}, of the channel [6]. In this context, we can estimate channel conductance as

$$G^{-1} = R = \frac{K_{\text{cell}}}{\kappa} = \rho K_{\text{cell}}, \tag{1}$$

where G is the conductance (in Siemens, S), R is the resistance (in Ω), κ is the conductivity of the electrolyte in the channel (in $\Omega^{-1}\,\text{m}^{-1}$) and ρ is the resistivity (in Ω m). For a macroscopic conductance cell, the constant K_{cell} is defined as l/A, where l is the length of the cell and A is the cross-sectional area. In an improvement over the work in [6], we calculate the cell constant of a channel as the sum of the contributions of n successive thin cross-sections:

$$K_{\text{cell}} \approx \sum_{i=0}^{n-1} \frac{||\boldsymbol{p}_{i+1} - \boldsymbol{p}_i||}{A_i}, \tag{2}$$

where $\boldsymbol{p}_{i+1} - \boldsymbol{p}_i$ is the vector indicating the direction of the longitudinal path at the i-th local cross-section of the channel, with area A_i. Our goal is to compute K_{cell} by using an improved analysis of the internal geometry of the channel. To this end, we discuss two algorithms: (*i*) the program TRAJECT, that calculates the trajectory of a point-like object passing through the pore of a channel, (*ii*) the program AREA, that computes the cross-sectional areas of the channel along the trajectory derived in (*i*). The $\{\boldsymbol{p}_i\}$ points along the trajectory in Eq. (2) are derived from TRAJECT, and the cross-sectional areas A_i at each of the $\boldsymbol{p}_i$ are computed by using AREA.

We assume that the electric field lines will be locally parallel to the longitudinal pore trajectory. Moreover, we assume that the contribution to the conductivity κ of the ion with largest mobility can be taken as that for the bulk solution outside the channel. In this work, conductances are predicted by using the conductivity $\kappa = 12.5\,\Omega^{-1}\,\text{m}^{-1}$ of a 1 M KCl solution as a reference [7]. Values for lower concentrations can be obtained by linear interpolation.The proposed model exhibits known, intrinsic limitations. In principle, a geometrical model of the conductance should work better in channels whose cross-sections are significantly larger than the typical cross-sections of solvated ions. Many biological channels, however, have minimum pore diameters comparable to the dimensions of a water molecule. For instance, the "head-to-head" (HH) conformer of gramicidin is believed to allow the passage of a single file of water molecules, [8,9] whereas some porins can accommodate only a few water molecules at the narrowest section [10,11]. In contrast, channels for the transport of anions (e.g. Cl^-) may allow no water molecules [12]. In addition, the transport of ions with large radii is expected to be constrained strongly by (and possibly perturb) the channel's geometry [6].

The use of a macroscopic model for calculating the conductance of a microscopic "cell" will likely cause systematic deviations from experimental data. Smart et al. [6] have proposed an improvement that employs a parametrization scheme that accounts for physical features of the channels. Such corrections improve results among channels that share similar structural characteristics. Here, we extend the work along two directions: (*i*) an improved methodology to compute the geometrical features of the channel, and (*ii*) the use of a single correction factor, applicable to all channels, that accounts for systematic deviations.

2.1. Algorithm for program TRAJECT

The program *TRAJECT* is used to calculate the trajectory of a *point-like object* passing through a pore. The channel structure is derived by adding hydrogens atoms to the available PDB coordinates. As a first approximation to a channel axis vector, we set:

$$\boldsymbol{v}_0 = \boldsymbol{p}_{\text{F}} - \boldsymbol{p}_I, \tag{3}$$

where $\boldsymbol{p}_{\text{I}}$ and $\boldsymbol{p}_{\text{F}}$ are the vectors for two conveniently chosen entry and exit points, respectively. Then, we calculate a first *tentative* point along the channel trajectory, $\boldsymbol{p}'_1$, obtained by taking a step of length "s" along the $\boldsymbol{v}_0$ direction:

$$\boldsymbol{p}'_1 = \boldsymbol{p}_0 + s\frac{\boldsymbol{v}}{||\boldsymbol{v}||}, \tag{4a}$$

where initially $\boldsymbol{v} = \boldsymbol{v}_0$ and $\boldsymbol{p}_0 = \boldsymbol{p}_I$. The s value sets the precision of the calculation. Next, we refine the position (from the tentative $\boldsymbol{p}'_1$ to the actual $\boldsymbol{p}_1$) by using a perpendicular plane to $\boldsymbol{v}$. The new trajectory point $\boldsymbol{p}_1$ lies on this plane, and is determined by selecting one of two possible methods:

(a) we minimize the sum of squared distances from the point $\boldsymbol{p}_1$ to the inner surface of the channel, as represented by the set of atomic spheres of the channel wall *intersected by the plane*, or
(b) we minimize the sum of squared distances from the point $\boldsymbol{p}_1$ to a set of atomic spheres found in *any direction*, within a certain cut-off window.

In both approaches, we have implemented analytical derivatives. The molecular surface of the channel is defined by using standard van der Waals radii [13]. The set of atoms used in the minimization algorithms above are selected by ensuring a reasonable, yet simple estimation of the *inner* surface of the channel. First, we select nuclei that lie within a specified cut-off distance from the tentative $\boldsymbol{p}'_1$. Second, we exclude any nucleus satisfying the first criterion but whose vector to $\boldsymbol{p}'_1$ is intersected by another atom's surface. This condition eliminates nuclei that would not be perceived as belonging to the inner surface of the channel when "seen" from $\boldsymbol{p}'_1$. The resulting set of atoms is used for minimizing according to method (b). For the minimization scheme (a), the set of atoms is further reduced to only those intersected by the cross-sectional plane at $\boldsymbol{p}'_1$.

Minimizations employ an iterative two-dimensional Newtwon–Raphson algorithm, using the local system of

coordinates of the transversal plane (here, "plane (1)"). The starting point for the iteration is the tentative point $\boldsymbol{p}'_1$. The minimization provides the "corrected" first trajectory point, $\boldsymbol{p}_1$, a point that is optimally centred at the local cross-section of the channel. From this point, we can now estimate a next tentative point $\boldsymbol{p}'_2$ by using the previous point $\boldsymbol{p}_1$ in Eq. (4a). Whenever this step is repeated along the trajectory, we write in general:

$$\boldsymbol{p}'_i = \boldsymbol{p}_{i-1} + s\frac{\boldsymbol{v}}{||\boldsymbol{v}||}, \tag{4b}$$

where the direction vector **v** is recalculated at every tentative trajectory point as:

$$\boldsymbol{v} = \boldsymbol{p}_{i-1} - \boldsymbol{p}_I. \tag{5}$$

Finally, the new tentative point $\boldsymbol{p}'_i$ and vector **v** define a new "plane (i)," on which the next trajectory point $\boldsymbol{p}_i$ is found by minimization. The process is repeated until the trajectory is determined to have exited the channel, by using the initial direction $\boldsymbol{v}_0$ and the final point. This approach can even be applied to irregular channels [14]. With an appropriate choice for the step length "s," we can produce a smooth trajectory, meandering along any desired channel.

The program *TRAJECT* has been tested on a series of "toy" models and experimental structures. Consider first the case in Fig. 1, consisting of a regular 40 Å-helix with 11 turns. On this model, we have constructed a number of trajectories and measured their quality in terms of the accumulated deviation, σ, for each trajectory point with respect to the central axis of the helix, (the latter can be taken as coinciding with $\boldsymbol{v}_0$). Due to the inherent symmetry of this helix, the cumulative deviation should approach zero in an optimized, very accurate trajectory path.

In a high-resolution calculation ($s = 0.1$ Å), the minimization method (a) above produces the trajectory in Fig. 1A, with a cumulative deviation $\sigma = 9.32$ Å. In constrast, the minimization method (b), produces the trajectory in Fig. 1B with $\sigma = 0.44$ Å, excluding the end points of the trajectory in both cases, (precision at the ends of the channel can be improved by simply choosing different initial and final points, see later). This result illustrates a general trend, as the minimization method (b) gives consistently the best trajectories for all channels.

The difference between the two methods can be easily understood in the case of a helical channel. When minimizing a sum of (squared) distances to atoms in the plane (i.e. method (a)), a trajectory point is "dragged away" from the channel axis towards the intersection of the transverse plane with the helical backbone. When the next point is analyzed, the new transversal plane will intersect nodes further away along the backbone, and thus the new point will be displaced towards these new nodes. As a result, the trajectory oscillates within the helix (cf. Fig. 1C). If the helical pitch is increased as in Fig. 1D, method (a) produces a very poor trajectory. In contrast, method (b) still produces a smooth trajectory, as illustrated in Fig. 1E.

Fig. 2 shows the resulting trajectories for a real channel, corresponding to the HH conformer of gramicidin. Here, the entry and exit point coordinates were selected from the axes of inertia, after displaying the PDB coordinates with a standard molecular modelling program [15]. For gramicidin, we used a 6.0 Å cut-off for selecting the ensemble of atoms to be

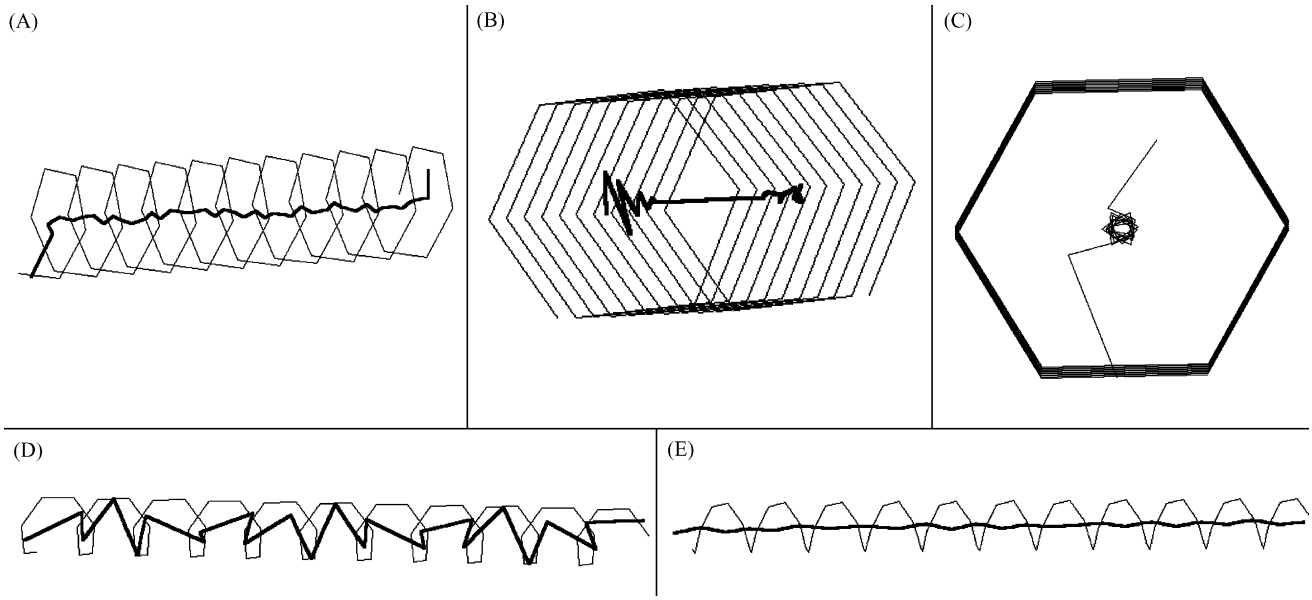

Fig. 1. Longitudinal trajectories for model helical pores. (A) Path derived by minimizing the square distance to the exposed van der Waals spheres found within a cross-sectional plane. (B) Path derived by minimizing the square distance to the exposed van der Waals spheres within a cut-off distance to the centre of the local transversal cross-section. (C) Longitudinal view of path A, showing the oscillatory trajectory of (A). (D) Same as path A, but for a "stretched" helix. The quality of the path diminishes when using this procedure. (E) Same as path B, but for a "stretched" helix. This method produces smoother paths for helices in various shapes.

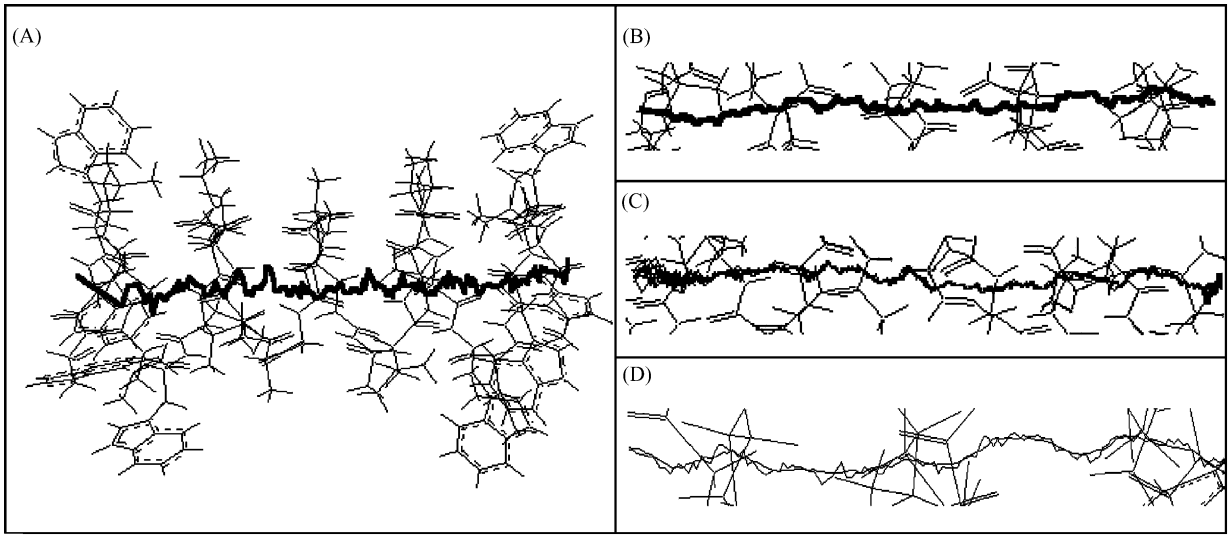

Fig. 2. Trajectories for the gramicidin channel in HH conformation. (A) Path derived by minimizing the square distance to the exposed van der Waals spheres within a cross-sectional plane. (B) Path derived by minimizing the square distance to the exposed van der Waals spheres within a cut-off distance to the local transversal cross-section. (C) Twelve superimposed trajectories, built using the approach (B). Each trajectory differs in the choice of initial point. (D) The smooth line corresponds to an average trajectory derived from the set of twelve in (C). The result is compared with the single trajectory in case (B).

included in the minimization. A high-resolution calculation ($s = 0.1$ Å) with minimization within the transversal plane (method (a)), produces the trajectory in Fig. 2A, with a deviation of $\sigma = 85.56$ Å from the central axis. When extending the minimization to a 6 Å window about the cross-sectional plane (method (b)), we obtain the smoother trajectory shown in Fig. 2B (with $\sigma = 69.70$ Å).

As expected, trajectories depend on the choice of the entry point $\boldsymbol{p}_1$. For this reason, an improved trajectory can be derived by averaging over a number of possible choices of $\boldsymbol{p}_1$. Fig. 2C shows the superimposed results for 12 trajectories of the HH gramicidin channel, whose initial points were located within a circumference with 0.3 Å radius, centred at one end of the channel axis. Note that the differences among trajectories are greatest at the ends of the channel. Fig. 2D compares a path averaged over the 12 individual trajectories with that of the single trajectory in Fig. 2B. This averaging diminishes the cumulative deviation to $\sigma = 65.20$ Å.

In summary, our results suggest that method (a) (without averaging) is practical only when dealing with near-cylindrical pores. This method produces a good trajectory for the anti-parallel double stranded (APDS) conformer of gramicidin [16], featuring two interwoven chains. For irregular channels, we employ method (b), involving "out-of-plane" minimization.

2.2. Algorithm for program AREA

Program *AREA* is used to compute the locally transversal cross-sectional areas associated with the paths computed by *TRAJECT*. At each point $\boldsymbol{p}_i$, we determine the plane perpendicular to the path vector $\boldsymbol{n} = \boldsymbol{p}_{i+1} - \boldsymbol{p}_i$ (cf. Eq. (2)). The cross-sectional area is then evaluated from the atoms intersected within each plane. The key steps in the algorithm are as follows:

(i) The area is computed by initially dividing the cross-section of the channel into a maximum of 720 triangles. These triangles are built by scanning the interior of the channel with radial lines starting from $\boldsymbol{p}_i$ as the origin (at angles of $\delta = 0.5$ degrees), and finding the intersections between these lines and the exposed atom surfaces. If two adjacent atoms intersect at a point "visible" from the origin, the areas associated with the triangles constitute the so-called "mode 0" contribution to the transversal area. The corresponding area is indicated in Fig. 3, for the case of a "toy" model of a generic cross-section.

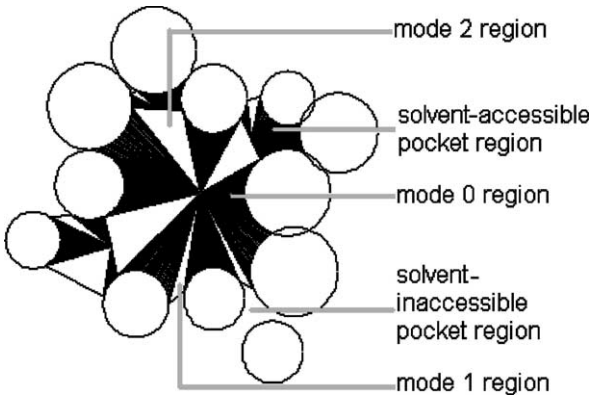

Fig. 3. Example of a transversal cross-section for a generic pore. The circles represent the cross-sections of the atomic van der Waals spheres defining the inner surface of the channel. The various contributions to the transversal area are indicated, see text.

(ii) In many channels, transversal cross-sections may not be completely delimited; they may exhibit small openings leading to pocket regions not "visible" from radial lines originating at $\boldsymbol{p}_i$. Whenever a line fails to intersect any of the atoms in the plane, the corresponding contributions to the area are denoted by "mode 1". Contributions of this type are shown in Fig. 3.

(iii) The program uses a "mode 2" contribution to the area (see Fig. 3) when the length ratio for the $(j-1)$th and jth radial segments is below a cut-off value. The program scans subsequent radial lines until the length ratio is again satisfied, and then calculates the area of the triangle.

(iv) "Pocket regions" lie beyond the white triangles corresponding to "mode 1" and "mode 2" areas. Their contributions are calculated by the same methods (i.e. modes 0, 1, 2) if the region is accessible to a spherical probe. Accessibility implies that the probe reaches the pocket from the inside of the channel. To produce triangles within the pocket regions, new radial lines are traced from the midpoint of the segment at the opening of the pocket (cf. Fig. 3).

The probe radius should be set in accordance with the *vdW* radii of the "naked" (i.e. unsolvated) ions. For ions having substantially different radii, the contribution of each would have to be calculated separately using an appropriate probe. In our case, we use KCl for calculating conductances, an electrolyte whose ions are similar in radii to that of a water molecule. For this reason, the regions accessible to a "naked" ion and the regions accessible to water are essentially equivalent within the context of this work. In practice, therefore, the same probe is used for K^+, Cl^-, and water, all of them represented by a standard spherical accessibility probe [17].

Upon completing the calculation at a given plane, the program proceeds to the next one until the last trajectory point is reached. As illustration, Fig. 4 shows the contributions to the area in representative cross-sections of real channels. Even in irregular pores such as the one in Fig. 4F, the method succeeds at defining a reasonable transversal cross-section for the channel.

2.3. Computation of cross-sectional areas and cell constants

A number of ion channels were analyzed with the algorithms above. The estimates of conductance, obtained from Eq. (2) take ca. 30 min on a PII-450 Mhz PC, using $s = 0.1$ Å steps. The channels considered exhibit the following characteristics:

- The transmembrane domain of phospholamban (code 1pln), [18] an ion channel in the sarcoplasmic reticulum of human cardiac tissue. This channel is selective for Ca^{2+} ions, but has measurable activity with K^+. The available entry "1pln" is a theoretical model.
- Gramicidin A, a polypeptide extracted from *Bacillus brevis*, appears usually as a dimer in the HH conformation (PDB code: 1grm) [19]. The dimer can insert itself into phospholipid membranes, and selectively transport monovalent cations.
- The potassium channel (KcsA) from *Streptomyces lividans* (code 1bl8) [20]. The channel regulates the transport of K^+, and it is also permeable to Na^+.
- The cholera toxin (code 2chb) [21], produced by the bacteria *Vibrio cholerae*, has the ability to form channels in lipid bilayers, due to the presence of its B subunit.
- The channel associated with the α-hemolysin toxin of *Staphylococcus aureus* (code 7ahl) [22]. The toxin causes cell death by allowing permeation of ions, water, and other small molecules.
- Porins are large trimeric proteins found in the outer membrane of Gram-negative bacteria. The channels known as OmpF (code 2omf) [23] and PhoE (code 1pho) [10] of *Escherichia coli*, OmpC (code 1iiv) [24] of *Salmonella typhimurium*, and porin (code 2por) [25] from *Rhodobacter capsulatus* are rather unselective diffusion pores, transporting molecules with mass below 600D. The LamB porins of *E. coli* (code 1mal) [26] and *S. typhi* (code 1mpr) [27] transport and bind selectively maltose and maltodextrins. The sucrose-specific porin ScrY from *S. typhimurium* (code 1a0s) [28] resembles the latter porins in some aspects, but differ in some key properties.

Excluded from our analysis were the cases of anion-specific transport channels [12] and channels that transport water molecules (e.g. aquaporins [11]). Despite their differences in transport mechanisms, these latter channels share the structural feature of being composed of several monomers, each one of which contributes a single pore. In contrast, cation transport channels feature a single pore delimited by the assembly of several monomeric units.

The programs *TRAJECT* and *AREA* were used to compute high-resolution ($s = 0.1$ Å) cross-sectional areas, path lengths, and the cell constants K_{cell} (Eq. (2)). As illustration, Fig. 5 shows the profile of computed transversal areas for the HH gramicidin channel as a function of the distance to the centre of the channel. This example represents a worst case, since the narrowness of the channel produces strong oscillations in cross-sections, once pocket regions are included. Fig. 5 contrasts the results obtained when using the optimal trajectory path (gray line) and the channel axis (black line). Although the latter produces the smoothest profile, the overall agreement is satisfactory. For the other channels considered, their larger pores produce smaller fluctuations in transversal area.

When calculating the cell constants for the cholera toxin B-subunit pentamer, HH gramicidin, APDS gramicidin, KcsA and phospholamban, we used both the computed trajectory and the channel axis. When including the pocket regions, we obtain the cross-sections accessible to the

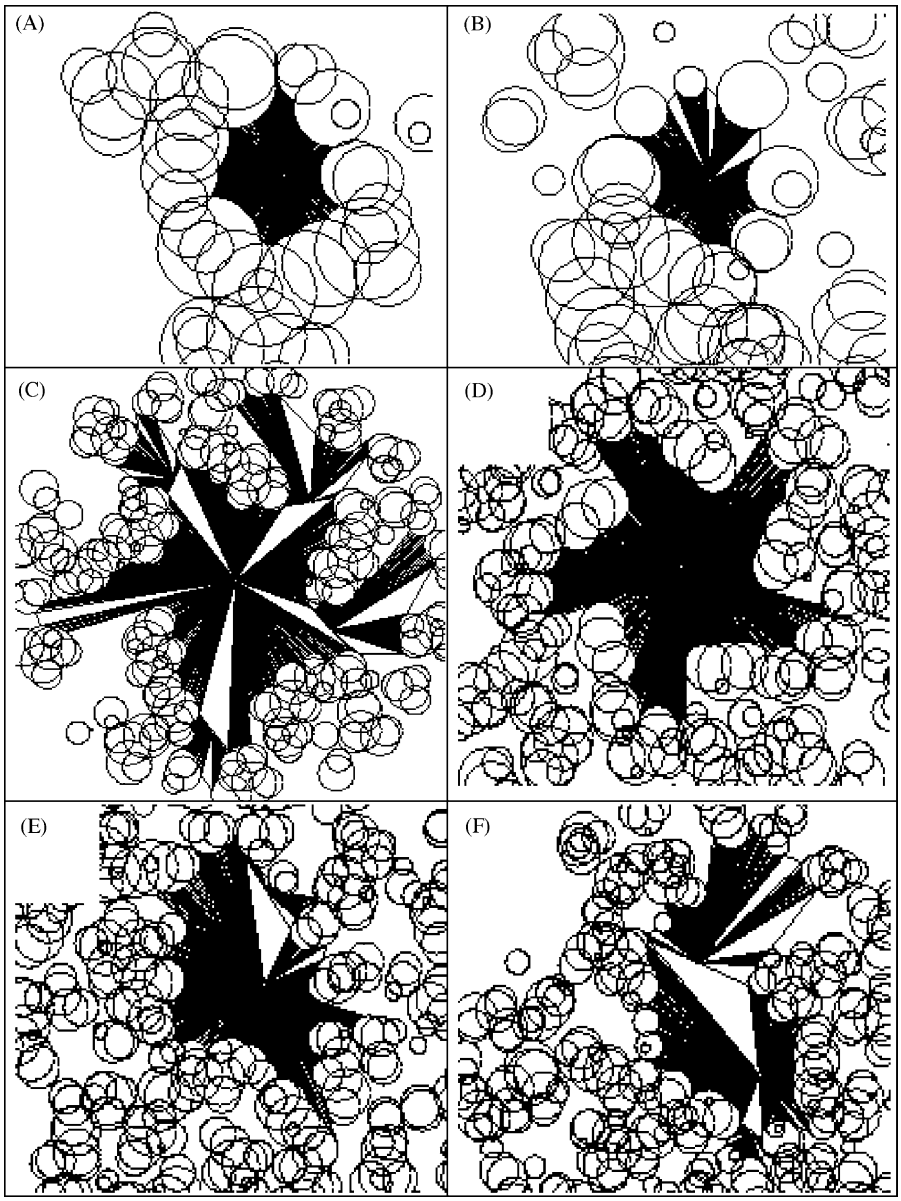

Fig. 4. Illustrative examples of cross-sections in various channel proteins. Cases (A) and (B) correspond to different transversal sections of gramicin A (1grm). Cases (C) and (D) are two different cross-sections of cholera toxin (2chb). Cases (E) and (F) correspond to representative cross-sections of the OmpF (2omf) and LamB (1mal) porins, respectively.

"naked" ion. This approach would underestimate the cell constant, since cations do maintain a degree of hydration within the channel; conversely, excluding pocket regions would overestimate the cell constant. In principle, these effects could be corrected by considering the cross-sections accessible to a *hydrated ion*. However, we did not find convenient to include a hydrated-ion probe, since the degree of hydration can differ from that in bulk solvent and indeed often varies along the channel pore (e.g. porins, potassium channels). Altogether, these four approaches span the range of values for the geometrical contribution to the Ohmic conductance. Since the main differences in K_{cell} value are due to the contributions of pocket regions, we have used only the channel axis to compute cross-sectional areas for the larger, more time-consuming cases (1mal, 1mpr, 2omf, 1pho, 1iiv, 2por, 1a0s, 7ahl).

In addition to the above approaches, we have also analyzed how the results depend on the definition of the inner van der Waals surface of the channel. To this end, we have recomputed the cross-sectional areas corresponding to "scaled" channels. These new pores are derived by multiplying the standard van der Waals radii by a scaling factor *f*, ranging from 0.80 to 1.20 [16]. As illustration, Fig. 6 depicts the various estimates of K_{cell} (in $Å^{-1}$) for the cholera toxin B-subunit pentamer channel, denoted by the curves (a), (b), (c), and (d). In particular, curve "a" provides an upper

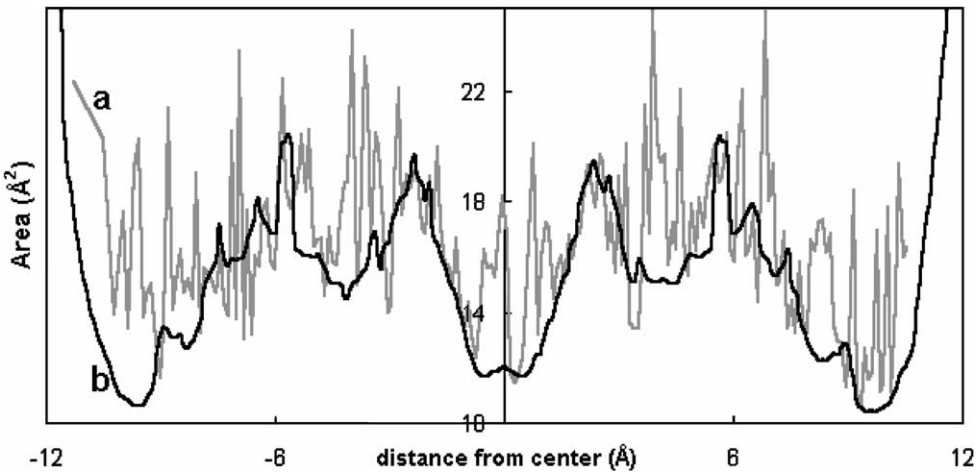

Fig. 5. Profile of cross-sectional areas for 1grm, as a function of the distance to the centre of the pore. Line (A) corresponds to the cross-sections that are transversal to the optimized trajectory. Line (B) corresponds to the cross-sections that are transversal to the channel axis. The calculated areas include the so-called "pocket regions."

estimate for the cell constant, with a reasonable upper bound at the narrow channel defined by $f = 1.10$. Similarly, curve (d) provides a lower estimate for the cell constant; a reasonable lower bound corresponds to the wider channel defined by $f = 0.90$, (see the figure caption regarding the details for each particular curve).

An additional refinement of the data is possible, by considering the fact that channels have different permeabilities for cations and anions. To this end, we have recalculated the electrolyte conductivities using ratios of experimental transport numbers. We assume that the conductivity of the more permeable ion is the same in the bulk and inside the channel. Then, the relation $t_+/t_- = \kappa_+/\kappa_-$ (where t_+ and t_- are the transport numbers of cations and anions, respectively) allows us to estimate the conductivity of the whole electrolyte in the channel:

$$\kappa^{\text{channel}} = \kappa_+^{\text{channel}} + \kappa_-^{\text{channel}} = \kappa_+^{\text{bulk}} + \kappa_+^{\text{bulk}} \left(\frac{t_-}{t_+}\right)^{\text{channel}}, \tag{6}$$

where $\kappa_+^{\text{channel}} \approx \kappa_+^{\text{bulk}}$ if the channel is more permeable to cations. The κ_+^{bulk} value is obtained from

$$\kappa^{\text{bulk}} = \kappa_+^{\text{bulk}} + \kappa_-^{\text{bulk}} = \kappa_+^{\text{bulk}} + \kappa_+^{\text{bulk}} \left(\frac{t_-}{t_+}\right)^{\text{bulk}}, \tag{7}$$

where $(t_-/t_+)^{\text{bulk}}$ is the ratio of experimental (bulk) transport numbers for K^+ and Cl^-. At infinite dilution, the ratio is 1.038 [29]. Analogous equations can be written for channels that are more permeable to anions.

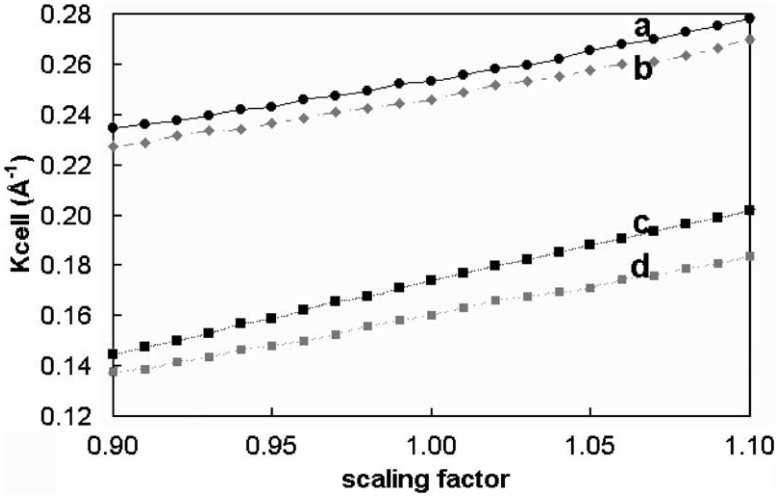

Fig. 6. Modelled cell constant K_{cell} for the 2chb channel, evaluated as a function of a factor, *f*, scaling the van der Waals radii. Curve (a) corresponds to a calculation using the simple channel axis as the path for the pore, and excluding pocket regions. Curve (b) uses the optimized trajectory as the pore path, and excludes pocket regions. Curve (c) shows the inclusion of pocket regions in case (a). Curve (d) shows the result of including pocket regions in case (b).

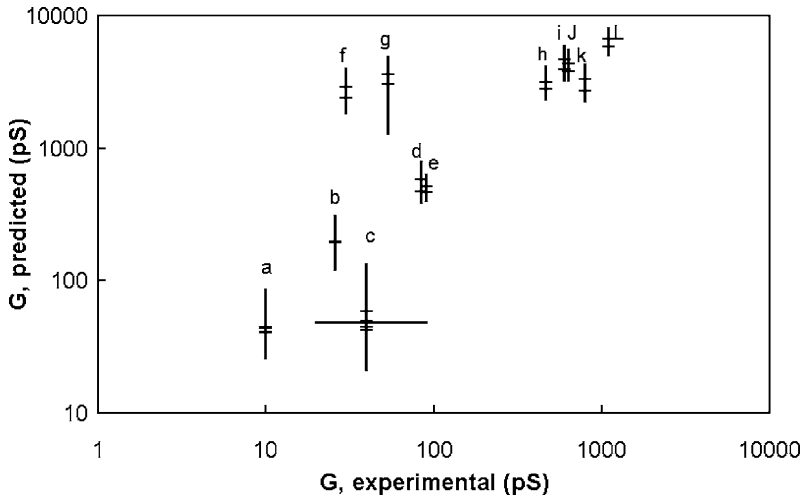

Fig. 7. Correlation between model and experimental conductances (in 10^{-12} S). The labels identify the following transport channels: (a) 1pln, (b) 1grm, (c) 1bl8, (d) 2chb, (e) 7ahl, (f) 1mpr, (g) 1mal, (h) 1a0s, (i) 1pho, (j) 2omf, (k) 1iiv, (l) 2por. The vertical lines represent the variations caused by scaling the atomic radii by ±10%. The dashes on each vertical line correspond to the estimates derived from K_{cell} curves such as those in Fig. 6 (for $f = 1$). The large horizontal bar for 1bl8 spans the experimental G-values associated with three known, distinct conducting states of this channel. Note that the model overestimates systematically the conductances by a factor of 5.

Table 1
Modelled Ohmic conductance (G_p) for KCl transport of various channels at 25 °C

Channel	1pln	1grm	1bl8	2chb[a]	7ahl[a]	1mpr[b]	1mal[b]	1a0s[b]	1pho[b]	2omf[b]	1iiv[b]	2por[b]
(KCl) (M)	0.05	0.5	0.2	0.1	0.1	1.0	1.0	1.0	1.0	1.0	1.0	1.0
k^{bulk} (Ω^{-1} m^{-1})	0.63	6.25	2.5	1.25	1.25	12.5	12.5	12.5	12.5	12.5	12.5	12.5
$(t_+/t_-)^{channel}$	∞	∞	∞	0.69 [34]	0.66 [35]	7 [36]	4.5 [37]	8.6 [31]	0.3 [37]	3.9 [37]	41 [37]	6.1 [37]
$k^{channel}$ (Ω^{-1} m^{-1})	0.31	3.07	1.23	1.08	1.06	7.01	7.5	6.85	8.28	7.71	6.28	7.14
G_{exp} (pS)	10 [39]	26 [40]	40 [41]	85 [34]	90 [35]	30 [36]	53 [42]	467 [31]	600 [43]	633 [37]	800 [37]	1100 [38]
min G_p (pS)[c]	26	121	21	386	403	1851	1279	2338	3214	3261	2269	5038
max G_p (pS)[d]	85	305	132	782	622	3956	4836	4121	5920	5510	4266	8043
av. G_p (pS)[e]	42	193	48	522	485	2607	3303	2968	4280	4070	2995	6222
av. G_p^u (pS)[f]	86	393	99	606	574	4649	5508	5418	6463	6603	5961	10895

[a] For these channels, conductances were measured at several pH values. For 2chb and 7ahl, the values given correspond to $pH = 6.5$ and 7.0, respectively.

[b] Experimental conductances given for 1mal, 2omf, 1pho, 2por, 1iiv, 1mpr, 1aos have been obtained by dividing the literature values by three, as they correspond to trimers [44].

[c] Minimum predicted values, min G_p, are derived from the K_{cell} estimate obtained with exclusion of pocket regions and a scaling factor $f = 1.10$.

[d] Maximum predicted values, max G_p, are derived from the K_{cell} estimate obtained with inclusion of pocket regions and a scaling factor of 0.90.

[e] The average predicted values, av. G_p, are derived from the averaged K_{cell} estimates corresponding to the scaling factor $f = 1.00$.

[f] No correction for ion selectivity (i.e. $\kappa^{channel} \equiv \kappa^{bulk}$ for both ions).

Fig. 7 compares the "predicted" model values (G_p) with the experimental ones (G_{exp}). Note that the experimental data do not correspond to uniform KCl concentrations. We have used the upper and lower bound estimates for K_{cell} to compute vertical error bars for the conductances in Eq. (1). Horizontal dashes in Fig. 7 represent the values of G associated with the estimates of K_{cell} using $f = 1.00$. The large horizontal bar for the KcsA channel (case "c") represents the range of experimental values for the accessible conducting states of this channel (presumably matched with different conformations). The results for all the channels considered are summarized in Table 1. For completeness, the analogous results calculated without transport number corrections are also included. This latter approach would be useful in cases where the selectivity of a channel is not known.

Table 1 confirms that an Ohmic model overestimates the conductance ($G_p > G_{exp}$) since specific interactions with the channel wall are omitted. However, the results in Fig. 7 suggests that the difference amounts to a rather uniform systematic deviation, Gp ∼ 5 Gexp. In other words, the present model retains some predictive power since it accounts for the general qualitative trend in conductance for the considered channels.

3. Conclusions

Given that the overestimates are systematic, the present geometrical approach can be valuable for modelling conductance in ion channels. The data in Fig. 7 provide a "standard

curve" from which qualitative predictions can be made. (It should also be mentioned that available experimental techniques do not use the same ranges of electrolyte concentration. Given that different channels have been studied with different approaches, trends extracted from experimental results should be employed carefully).

Our work sheds light on the best possible performance that can be expected from an Ohmic model of conductance. On the one hand, we have shown that pores are not uniform, but rather exhibit large fluctuations in transversal cross-sections (cf. Fig. 4). In turn, these areas can vary largely on account of ion accessibility. In addition, important variations in conductance result also from the "fuzziness" in the definition of the inner channel wall (as shown by the results obtained with scaled van der Waals radii). The present deviations between the model G_p values and the experimental ones are clearly due to the physical limitations of the model; they are not associated with the methodology used to compute the cell constants.

There are several causes for the observed systematic deviations. Firstly, a protein channel is not a rigid structure; it exhibits both thermal fluctuations and distortions during ion transport. Secondly, the conductivity of an electrolyte in a channel is smaller than that in bulk solution [30]. This is to be expected given that ion mobility is strongly reduced by geometrical confinement in the pore, as well as by specific interactions with the channel wall. Thirdly, the solvent inside the channel has different mobility; in cases, it may resemble the bulk solvent at lower temperatures.

Aside from the KcsA (1bl8) channel whose structure cannot positively be assigned to one of its three conducting states, the maltoporins of *E. coli* (1mal) and *S. typhi* (1mpr) show large deviations from the trend observed in the rest of the channels. These deviations can be understood if we consider that the latter porins differ markedly from "generic" porins in that they lack a transversal electric field that favours diffusion of polar molecules. In addition, their conductances decrease upon the introduction of maltose or maltodextrins into the binding site (located at the most constricted point of the channel), a region which also features strongly bound water molecules [27]. In contrast, the sucrose-specific porin (1a0s) is similar to generic diffusion-controlled porins in its properties [31]. Since the present geometric model cannot incorporate these particular differences, it is not surprising that both the 1mal and 1mpr channels are deviant in Fig. 7. Therefore, it emerges from the results that the present approach is more adequate for the modelling of rather unselective pores, i.e. those where the interactions between the ion and the channel are minimal [32].

While the results in Table 1 assume that the conductivity of the most permeable ion is the same in the channel and in the bulk, this approach does incorporate the correct ratio of conductivities between cations and anions. Provided that the data for transport numbers is available, this correction is straightforward. In the case of cation-transport channels, the correction is essential in order to avoid overestimating the number of charge carriers. Nevertheless, the small qualitative improvement using this correction would suggest that electrostatic effects, absent in our approach, are more important than the steric effects associated with the shape of the channel.

Further improvements to the model can take several forms. As suggested in [6], conductivities can be rescaled by taking into account the diffusion coefficients of ions and water. An improved model should also take into account specific electrostatic and hydrophobic interactions associated with the amino acid residues exposed to the inner channel wall. Nevertheless, the present approach provides a simple and expedient route to generate estimates of conductance. An analysis of the mechanism for ion transport and selectivity are beyond the scope of the model, and should be studied with detailed computer simulations [2,3,30,33].

Acknowledgements

GAA acknowledges support from the Natural Sciences and Engineering Research Council (NSERC) and the Canada Research Chairs' Program. JS acknowledges support from an NSERC USRA.

References

[1] A. Ishijima, T. Yanagida, Single molecule nanobioscience, Trends Biochem. Sci. 26 (2001) 438–444.
[2] S. Bernèche, B. Roux, Energetics of ion conduction through the K+ channel, Nature 414 (2001) 73–77.
[3] M.S.P. Sansom, I.H. Shrivastava, K.M. Ranatunga, G.R. Smith, Simulations of ion channels—watching ions and water move, Trends Biochem. Sci. 25 (2000) 368–374.
[4] B. Hille, Ionic Channels of Excitable Membranes, 2nd Edition, Sunderland, MA, 1992.
[5] M.S.P. Sansom, I.D. Kerr, Transbilayer pores formed by β-barrels: molecular modeling of pore structures and properties, Biophys. J. 69 (1995) 1334–1343.
[6] O.S. Smart, J. Breed, G.R. Smith, M.S.P. Sansom, A novel method for structure-based prediction of ion channel conducance properties, Biophys. J. 72 (1997) 1109–1126.
[7] N.J. Selley, Experimental Approach to Electrochemistry, Edward Arnold, London, 1977.
[8] R.R. Ketchem, W. Hu, T.A. Cross, High-resolution conformation of gramicidin-A in a lipid bilayer by solid-state NMR, Science 261 (1993) 1457–1460.
[9] R. Pomès, B. Roux, Free energy profiles for H^+ conduction along hydrogen-bonded chain for water molecules, Biophys. J. 75 (1998) 33–40.
[10] S.W. Cowan, et al., Crystal structures explain functional porperties of two *E. Coli* porins, Nature 358 (1992) 727–733.
[11] H.X. Sui, et al., Structural basis of water-specific transport through the AQP1 water channel, Nature 414 (2001) 872–878.
[12] R. Dutzler, et al., X-ray structure of a CIC chloride channel at 3.0 Å reveals the molecular basis of anion selectivity, Nature 415 (2002) 287–294.
[13] A. Gavezzotti, The calculation of molecular volumes and the use of volume analysis in the investigation of structured media and of solid-state organic reactivity, J. Am. Chem. Soc. 105 (1983) 5220–5225.

[14] R.O. Fox, F.M. Richards, A voltage-gated ion channel model inferred from the 1amt crystal structure of alamethicin at 1.5 Å resolution, Nature 300 (1982) 325–350.
[15] Hyperchem 4.0, 1994, Hypercube Inc., Waterloo, Canada.
[16] G.A. Arteca, D.R. Van Allen, Three-dimensional lipophilicity characterization of molecular pores and channel-like cavities, J. Mol. Graphics 14 (1996) 235–242.
[17] M.L. Connolly, Solvent-accessible surfaces of proteins and nucleic acids, Science 221 (1983) 709–713.
[18] P. Herzyk, R.E. Hubbard, Using experimental information to produce a model of the transmembrane domain of the ion channel phospholamban, Biophys. J. 74 (1998) 1203–1214.
[19] A.L. Lomize, V.Y. Orekhov, A.S. Arseniev, Refinement of the spatial structure of the gramicidin A transmembrane ion-channel, Biol. Membr. (USSR) 18 (1992) 182–200.
[20] D.A. Doyle, et al., The structure of the potassium channel: molecular basis of K^+ conduction and selectivity, Science 280 (1998) 69–77.
[21] E.A. Merritt, et al., Structural studies of receptor binding by cholera toxin mutants, Protein Sci. 6 (1997) 1516–1528.
[22] L. Song, et al., Structure of staphylococcal alpha-hemolysin, a heptameric transmembrane pore, Science 274 (1996) 1859–1866.
[23] S.W. Cowan, et al., The structure of OmpF porin in a tetragonal crystal form, Structure 3 (1995) 1041–1050.
[24] A. Arockiasamy, S. Krishanswamy, Homology based model of *Salmonella typhi* OmpC and its immunological implications, J. Biosci. 20 (1995) 235–243.
[25] M.S. Weiss, G.E. Schulz, Structure of porin refined at 1.8 Å resolution, J. Mol. Biol. 227 (1992) 493–509.
[26] T. Schirmer, T.A. Keller, Y.F. Wang, J.P. Rosenbusch, Structural basis for sugar translocation through maltoporin channels at 3.1 Å resolution, Science 267 (1995) 512–514.
[27] J.E.W. Meyer, M. Hofnung, G.E. Schulz, Structure of maltoporin from *Salmonella typhimurium* ligated with a nitrophenyl-maltotrioside, J. Mol. Biol. 266 (1997) 761–775.
[28] D. Forst, W. Welte, T. Wacker, K. Diederichs, Structure of the sucrose-specific porin ScrY from *Salmonella typhimurium* and its complex with sucrose, Nat. Struct. Biol. 5 (1998) 37–46.
[29] I.N. Levine, Physical Chemistry, 4th Edition, New York, NY, 1995.
[30] M.S.P. Sansom, Models and simulations of ion channels and related membrane proteins, Curr. Opin. Struct. Biol. 8 (1998) 237–244.
[31] K. Schülein, K. Schmid, R. Benz, The sugar-specific outer membrane channel ScrY contains functional characteristics of general diffusion pores and substrate-specific porins, Mol. Microbiol. 5 (1991) 2233–2241.
[32] M.S.P. Sansom, I.D. Kerr, J. Breed, R. Sankararamakrishnan, Water in channel-like cavities: structure and dynamics, Biophys. J. 70 (1996) 693–702.
[33] D.P. Tieleman, H.J.C. Berendsen, A molecular dynamics study of the pores formed by *Escherichia Coli* OmpF Porin in a fully hydrated palmitoyloleoylphosphatidylcholine bilayer, Biophys. J. 74 (1998) 2786–2801.
[34] O.V. Krasilnikov, J.N. Muratkhodjaev, S.F. Voronov, Y.V. Yezepchuk, The ionic channels formed by cholera toxin in planar bilayer lipid membranes are entirely attributable to its B-subunit, Biochim. Biophys. Acta. 1067 (1991) 166–170.
[35] G. Menestrina, Ionic channels formed by *Staphylococcus aureus* alpha-toxin: voltage-dependent inhibition by divalent and trivalent cations, J. Membr. Biol. 90 (1986) 177–190.
[36] K. Schülein, R. Benz, LamB (maltoporin) of *Salmonella typhimurium*: isolation, purification and comparison of sugar binding with LamB of *Escherichia coli*, Mol. Microbiol. 4 (1990) 625–632.
[37] R. Benz, A. Schmid, R.E.W. Hancock, Ion selectivity of gram-negative bacteria, J. Bacteriol. 162 (1985) 722–727.
[38] R. Benz, D. Woitzik, H.T. Flammann, J. Weckesser, Pore forming activity of the major outer membrane protein of *Rhodobacter capsulatus* in lipid bilayer membranes, Arch. Microbiol. 148 (1987) 226–230.
[39] R.J. Kovacs, M.T. Nelson, H.K.B. Simmerman, L.R. Jones, Phospholamban forms Ca^{2+} selective channels in lipid bilayers, J. Biol. Chem. 263 (1988) 18364–18368.
[40] D.W. Urry, et al., Shortened analog of the gramicidin A channel argues for the doubly occupied channel as the dominant conducting state, Biochim. Biophys. Acta. 775 (1984) 115–119.
[41] H. Schrempf, A prokaryotic potassium ion channel with two predicted transmembrane segments from *Streptomyces lividans*, EMBO J. 14 (1995) 5170–5178.
[42] R. Benz, A. Schmid, T. Nakae, G.H. Vos-Scheperkeuter, Pore formation of LamB of *Escherichia coli* in lipid bilayer membranes, J. Bacteriol. 165 (1986) 978–986.
[43] R. Benz, R.P. Darveau, R.E.W. Hancock, Outer membrane protein PhoE from *Escherichia coli* forms anion-selective pores in lipid bilayer membranes, Eur. J. Biochem. 140 (1984) 319–324.
[44] B.K. Jap, P.J. Walian, Biophysics of the structure and function of porins, Q. Rev. Biophys. 23 (1990) 367–403.